Measurements of F_2 and the total photon-proton cross sections at low x and low Q^2

Vincenzo Monaco[1]

Università di Torino, INFN, Via Pietro Giuria 1, 10125 Torino, Italy

On behalf of the H1 and ZEUS Collaborations

Abstract. The HERA measurements of the proton structure function F_2 at low Q^2 and very low values of the Bjorken variable x are presented. These measurements cover the transition region between the photoproduction limit ($Q^2 = 0$) and the DIS regime at $Q^2 > 1$ GeV^2. Whereas the behaviour of F_2 at moderate and high Q^2 is described by DGLAP evolution, in the low Q^2 region the F_2 behaviour can be described by phenomenological models inspired by Regge theory and the Vector Dominance Model.

1 Introduction

One of the early results from HERA was the discovery that the proton structure function F_2 is characterized by a steep rise with decreasing values of the Bjorken variable x [1,2]. This behaviour persists at low Q^2 values of the order of $Q^2 \sim 1.5$ GeV^2 [3,4] and can be interpreted as a purely perturbative phenomenon in terms of an increase of the gluon (xg) and sea quark ($x\bar{q}$) densities when smaller and smaller values of x are probed. Glück, Reya and Vogt (GRV) [5] predicted this behaviour well before the first HERA measurements; in their model the parton distributions are assumed to be non-singular (valence-like) at a very low Q^2 starting scale ($Q_0^2 \simeq 0.34$ GeV^2). The rise of xg and $x\bar{q}$ with decreasing x at higher Q^2 is generated dynamically via the DGLAP [6] evolution.

The proton structure function F_2 is related to the total virtual photon-proton cross section $\sigma_{tot}^{\gamma^* p}$ through the following relation, valid at low x and low Q^2

$$\sigma_{tot}^{\gamma^* p}(W, Q^2) \simeq \frac{4\pi^2\alpha}{Q^2} F_2(x, Q^2) \ , \qquad (1)$$

where $W^2 \simeq Q^2/x$ is the squared center of mass energy of the $\gamma^* p$ system.

From (1) it follows that a measurement of $F_2(x, Q^2)$ is equivalent to a measurement of the total cross section $\sigma_{tot}^{\gamma^* p}(W, Q^2)$, and that the rise of the structure function F_2 with decreasing x at moderate and high Q^2 and at low x corresponds to a rise of the total cross section with W at high values of W.

The W dependence of $\sigma_{tot}^{\gamma^* p}$ is shown in Fig. 1, where a partial compilation of measured cross sections is plotted as a function of W^2 for different Q^2 bins. The steep W dependence of the cross section at high and moderate Q^2 is well described by global next-to-leading order (NLO) perturbative QCD (pQCD) fits (the prediction of the MRS(R1) [7] parameterization is shown in Fig. 1). The

photoproduction cross section at $Q^2 = 0$, shown in the same figure, exhibits a much softer W dependence.

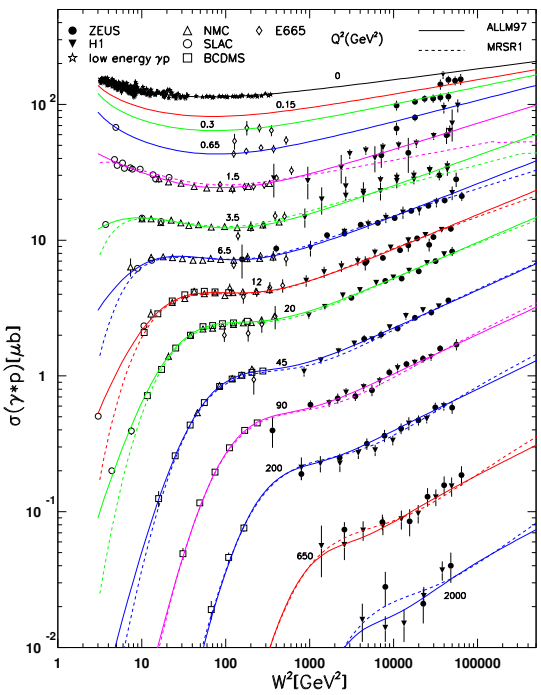

Fig. 1. Total $\gamma^* p$ cross section as a function of the $\gamma^* p$ center-of-mass energy in different bins of Q^2. The curves represent the ALLM97 [13] (*full line*) and the MRS(R1) [7] (*dotted line*) parameterizations. The points are data from H1, ZEUS and fixed target experiments

As shown by Donnachie and Landshoff (DL) [8] the W dependence of the photoproduction cross section is similar to the W dependence of the cross section of hadronic processes, described by a two-component Regge parameterization

$$\sigma_{tot}^{\gamma p}(W) = A_{IR}(W^2)^{\alpha_{IR}-1} + A_{IP}(W^2)^{\alpha_{IP}-1} \,, \tag{2}$$

where IR and IP denote the Reggeon and Pomeron contributions, with intercepts $\alpha_{IR} \simeq 0.5$ and $\alpha_{IP} \simeq 1.08$ respectively. At high W, where the Reggeon term is negligible, the energy dependence of the total cross section can be parameterized as $\sigma_{tot}(W) \propto W^{2\lambda}$, with $\lambda = 1 - \alpha_{IP}$ small and close to 0 in the photoproduction limit. Conversely, the behaviour of the DIS data with $Q^2 > 1$ GeV^2 at high W corresponds to a much higher effective power λ (between 0.2 and 0.4).

A transition between the different W dependences of the cross section in the two regimes is expected. One of the reasons for expecting new phenomenology in this region comes from the observation that the total photoproduction cross

section is finite; this, because of (1), implies that $F_2 \to 0$ as $Q^2 \to 0$, which entails strong scaling violations at low Q^2. Therefore, the description of the structure functions based on pQCD, which still works at a Q^2 scale of a few GeV^2, should fail at lower Q^2. It is interesting to see down to which low Q^2 value the NLO DGLAP formalism can be extended; at very low Q^2, however, pQCD predictions are not reliable at all and non-perturbative models have to be used.

At HERA, low Q^2 values correspond to very low values of x, where the average longitudinal distance travelled by the hadronic fluctuation of the photon in the proton rest frame ($l \sim 1/(2m_N x)$) is much longer than the target size. The ep scattering can be viewed as the interaction of a color dipole $q\bar{q}$ with the proton and the soft Regge-like behaviour of the photoproduction cross section is expected to hold also at finite but low values of Q^2. However, the Regge formalism can not be pushed to too high Q^2 values without introducing hard contributions.

The question is at which Q^2 and x values the behaviour of the structure function changes from being described by perturbative QCD to being dominated by non-perturbative contributions. Different models and parameterizations exist to interpolate between the soft and hard behaviour of the cross section [9–14].

Experimental methods

The structure function F_2 and the cross section $\sigma_{tot}^{\gamma^* p}$ have been measured in the transition region using e^+p collisions from the 1995-1997 HERA runs.

The 4-momentum transfer squared, Q^2, is related to the energy E'_e and the angle ϑ'_e of the scattered positron by

$$Q^2 = 4E_e E'_e \cdot \sin^2 \frac{\vartheta'_e}{2} , \tag{3}$$

where ϑ'_e is measured with respect to the direction of the positron beam and E_e is the positron beam energy. The limited angular acceptance of the main calorimeters of H1 and ZEUS fixes the lowest Q^2 to $\sim$ 1.5 GeV^2. In order to measure F_2 at lower values of Q^2, the final state positron must be identified at very small scattering angles ϑ'_e or the beam energy E_e must be reduced.

"Shifted Vertex" runs have been provided by HERA in 1995; in these runs the nominal interaction vertex was shifted in the proton beam direction by +70 cm, thereby increasing the angular acceptance of the detectors to smaller positron scattering angles. Both the H1 and ZEUS experiments have measured F_2 using data collected in these runs, extending the coverage of the kinematic plane down to Q^2 values of $\sim$ 0.35 GeV^2 (ZEUS) [15] and $\sim$ 0.6 GeV^2 (H1) [16].

In 1995 ZEUS extended the kinematic acceptance to low angles by installing two small beam pipe calorimeter modules (BPC) on two sides of the beam pipe at $\sim$ 3 m from the interaction point in the rear direction. Each module is a tungsten-scintillator sampling calorimeter, with an energy resolution of $\Delta E/E = 17\%/\sqrt{E}$. The BPC acceptance is $18 \leq \vartheta'_e \leq 32$ mrad. Data collected in 1995 with the BPC were used for the measurement of F_2 [17] in the kinematic range $0.11 \leq Q^2 \leq 0.65$ GeV^2 and $2 \times 10^{-6} \leq x \leq 6 \times 10^{-5}$.

Another method to extend the measurement of F_2 to lower Q^2 makes use of ep events with photons radiated collinear to the incident positron, resulting in an effective beam energy E_e reduced with respect to "non-radiative events". This method allows extension of the detector acceptance to low values of Q^2 in a complementary higher x range with respect to the BPC and shifted vertex measurements, but it suffers by large statistical and systematic errors.

The typical systematic error of the Shifted Vertex and BPC analyses is between 6 and 12 %, depending on the bin. The statistical errors are much lower.

2 Phenomenological analysis of the results

The results of the F_2 measurements based on the 1995 data are shown in Fig. 2 in Q^2 bins between $Q^2 = 0.11$ and 6.0 GeV^2. The results from the Shifted Vertex runs are labeled as H1 SVX95 [16], ZEUS SVX95 [15] those from BPC as ZEUS BPC95 [17]; some points from previous ZEUS analyses and from the E665 experiment [18] are also shown. The curves are the parameterizations from two fits of the ZEUS data based on non-perturbative models (ZEUSREGGE) and on NLO pQCD (ZEUSQCD). The data indicate that the rise of F_2 with decreasing x is prominent for values of $Q^2 > 1$ GeV^2, but becomes less steep for smaller Q^2 values.

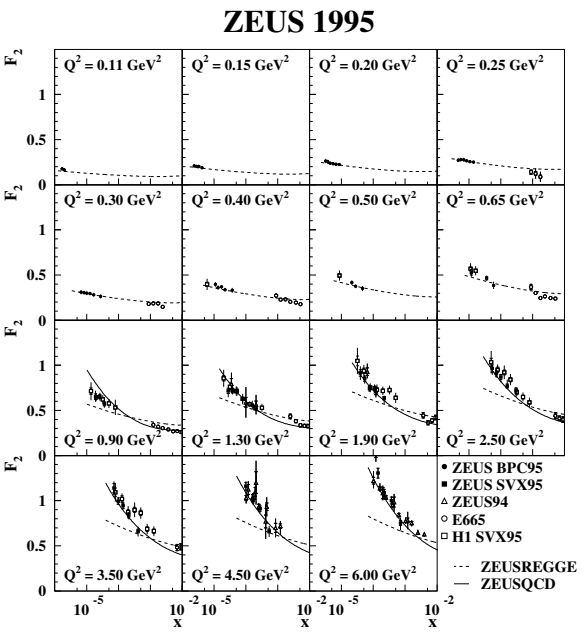

Fig. 2. $F_2(x, Q^2)$ at low Q^2 from "Shifted Vertex" runs (H1 SVX95 and ZEUS SVX95), ZEUS BPC and E665 data. The curves are described in the text

Figure 3 shows the cross section as a function of W^2 derived from the measured F_2 using (1). The two curves shown are the predictions of Donnachie and Landshoff (DL) [8] and of GRV94 [5]. The DL model describes the W dependence of the data at very low values of Q^2, but above $Q^2 = 0.65$ GeV^2 it predicts a shallower rise of the cross section than the data exhibit. The increasing rise of $\sigma_{tot}^{\gamma^* p}$ with W^2 for Q^2 values above 1 GeV^2 is described by the GRV94 curves.

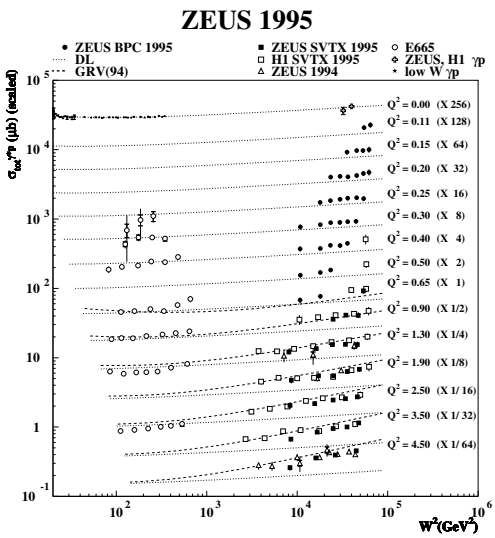

Fig. 3. The total $\gamma^* p$ cross section, $\sigma_{tot}^{\gamma^* p}$, as a function of W^2 for different Q^2 bins. Low Q^2 DIS measurements and photoproduction cross sections [20] are compared with the predictions of DL (*dotted line*) and GRV94 (*dashed line*)

In [15], a simplified Generalized Vector Dominance Model (GVDM) [19] approach was used to parameterize the Q^2 dependence of the cross section in the BPC range; in the fit described in [15] the longitudinal $\gamma^* p$ cross section is neglected, while the transverse cross section $\sigma_T(W^2, Q^2)$ is related to the corresponding cross section at $Q^2 = 0$, $\sigma_0(W^2)$, by

$$\sigma_T(W^2, Q^2) = \frac{M_0^2}{M_0^2 + Q^2} \sigma_0(W^2) \ , \tag{4}$$

where only the contribution from continuum vector states from a cut off mass M_0^2 has been kept. A fit of the BPC F_2 points to (4) gives $M_0^2 = 0.53$ GeV^2.

The W dependence of $\sigma_0(W^2)$ is parameterized by Regge theory through (2). The Q^2 and W dependence of the cross section $\sigma_{tot}^{\gamma^* p}$ used in the ZEUSREGGE fit is obtained by combining (2) and (4)

$$\sigma_{tot}^{\gamma^* p}(W^2, Q^2) = \left(\frac{M_0^2}{M_0^2 + Q^2} \right) \left(A_{IR} (W^2)^{\alpha_{IR} - 1} + A_{IP} (W^2)^{\alpha_{IP} - 1} \right) \ . \tag{5}$$

The ZEUS BPC data and low W photoproduction data from fixed target experiments [20] were fitted to (5), with A_{IR}, A_{IP} and α_{IP} left as free parameters. The intercept of the Pomeron is determined to be $\alpha_{IP} = 1.097 \pm 0.002$, compatible with the value of the DL fit. The fit result is shown in Fig. 2; the ZEUSREGGE fit gives a good description of the low Q^2 data in the BPC region $Q^2 \leq 0.65$ GeV^2, but at larger Q^2 the curves fall below the data.

The continuous curve in Fig. 2 (ZEUSQCD) is the result of a NLO QCD fit to the ZEUS data with $Q^2 > 1$ GeV^2; data from the NMC [21] and the BCDMS [22] experiments with $W^2 > 10$ GeV^2, not shown in Fig. 2, are also included to constrain the fit at high x. The details of the fit are described in [15]. The NLO DGLAP evolution equations are solved in the $\overline{\rm MS}$ scheme. The input scale is chosen to be $Q_0^2 = 7$ GeV^2, and backward evolution is performed to fit the data with $Q^2 < Q_0^2$. The quality of the fit is good (the χ^2 is 1474 for 1120 data points and 11 free parameters) as can be seen in Fig. 2, where the resulting F_2 is shown together with the measured values.

Figure 4 shows the gluon (xg) and singlet ($x\Sigma$) distributions obtained from the fit as a function of x for Q^2 at 1, 7 and 20 GeV^2. At the smallest Q^2 the gluon distribution is almost flat and compatible with zero, while the quark singlet distribution is still rising at small x.

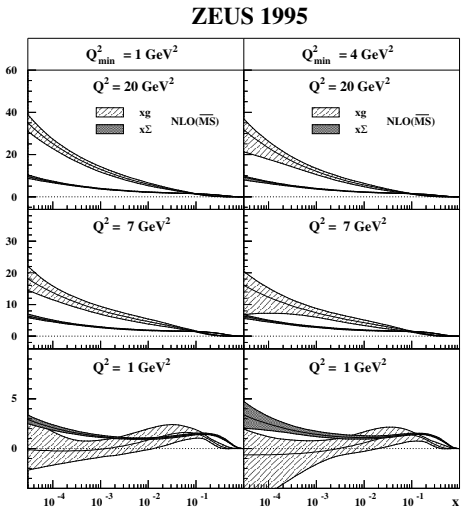

Fig. 4. The quark singlet momentum distribution $x\Sigma$ (*shaded*), and the gluon momentum distribution xg (*hatched*), as a function of x at $Q^2 = 1$, 7 and 20 GeV^2 from the ZEUS QCD fit. The left-hand plots show the results of the fit including data with $Q^2 > 1$ GeV^2; the results in the right-hand plots include data with $Q^2 > 4$ GeV^2. The error bands correspond to the quadratic sum of all the error sources

The quark singlet distribution is dominated at low x by the contribution from the $q\bar{q}$ sea distribution xS, and its evolution in Q^2 is coupled to that of the

gluons. It seems rather unphysical that the gluon does not drive the sea evolution at low Q^2; this behaviour (also observed, for instance, in the result of the fit by Martin et al. (MRST) [23]) is incompatible with the hypothesis that the rapid rise in F_2 is driven by the rapid increase of the gluon density at small x induced by parton splitting. However, no breakdown of the technical validity of the NLO QCD fit has been found in the kinematic range explored; the experimental data are well described down to $Q^2 \sim 1$ GeV^2.

The low x behaviour of F_2 as a function of x and Q^2 can be quantified through the slopes $d\ln F_2/d\ln(1/x)$ at fixed Q^2 and $dF_2/d\ln Q^2$ at fixed x.

The slope $\lambda_{eff} = d\ln F_2/d\ln(1/x)$, shown in Fig. 5, is extracted by fitting the data at fixed Q^2 to the form $F_2 = Ax^{-\lambda_{eff}}$, equivalent to the parameterization $\sigma_{tot}^{\gamma^* p}(Q^2, W^2) = A' \cdot W^{2\lambda_{eff}}$ for the total cross section. The slope λ_{eff} at $Q^2 < 1$ GeV^2 is compatible with the Q^2-independent Regge prediction $\lambda = 1 - \alpha_{IP} \simeq 0.1$, while at higher Q^2 it gradually increases with Q^2. This tendency at high Q^2 is not followed by the dominant Pomeron term of soft Regge phenomenology, but is qualitatively described by pQCD fits. As an example, the prediction of the GRV94 parameterization and the result of the ZEUS QCD fit for $Q^2 > 1$ GeV^2, obtained using the same x range of the data, are shown in Fig. 5.

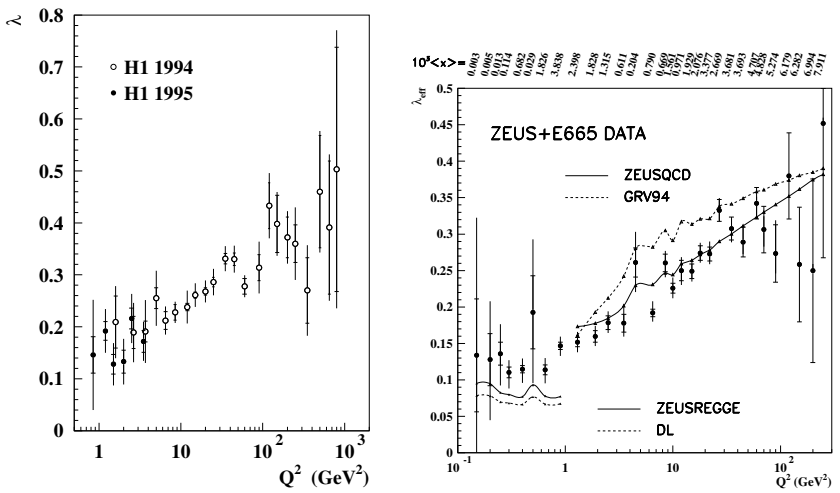

Fig. 5. The slope $\lambda_{eff} = d\ln F_2/d\ln(1/x)$ as a function of Q^2 as determined by a fit to H1 (**left**) and ZEUS (**right**) data

The logarithmic slope $dF_2/d\ln Q^2$ is derived from the data by fitting $F_2 = a + b\ln Q^2$ in bins of fixed x. The slope $dF_2/d\ln Q^2$ at low x is dominated by the convolution of the splitting function P_{qg} and the gluon density ($dF_2/d\ln Q^2 \propto \alpha_S P_{qg} \otimes xg$), and can be considered as a quantitative evaluation of the scaling violations caused by gluon bremsstrahlung and quark pair creation.

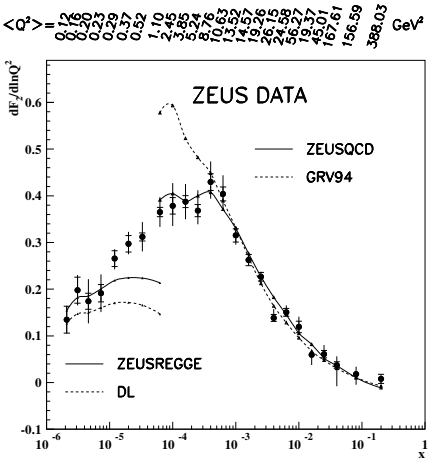

Fig. 6. The slope $dF_2/d\ln Q^2$ as a function of x as determined by the fit of ZEUS data

The dependence of the logarithmic Q^2 slope on x, as determined from the fit of the ZEUS data, is shown in Fig. 6, where for each bin the mean value of Q^2 is also shown. For values of x down to 3×10^{-4} the slope increases as x decreases. In this x range, where the mean values of Q^2 are high enough that pQCD fits are expected to be reliable, the ZEUS QCD fit and the GRV94 parameterization are in good agreement with the data. The trend of the slope in this region reflects the rapid increase of the gluon density with decreasing values of x obtained by the same ZEUS QCD fits.

At lower values of x and Q^2 the slope has the opposite behaviour, it decreases for decreasing x, with a "turn-over" at $x \sim 3 \times 10^{-4}$ and at a mean Q^2 value of a few GeV^2. It should be noticed that the exact position of the "turn-over" could depend on the correlations between the x and Q^2 values of the data points included in the fit. In the same Q^2 range the slope determined from fixed-target data continues to increase with decreasing values of x, but these data are at larger values of x.

The parameterization of DL and the ZEUSREGGE fit describe the x dependence of the slope only at very low values of x. As shown by the result of the ZEUS QCD fit, the standard NLO DGLAP equations are able to describe the behaviour of the slope down to $Q^2 \sim 1$ GeV^2.

It is not surprising that the GRV94 parameterization, obtained by a fit not constrained by data at low Q^2, does not follow the turn-over of the slope between $Q^2 \sim 1$ and $Q^2 \sim 10$ GeV^2; in this region the evolution of the sea and gluon distributions predicted by the DGLAP equations depends strongly on the shape of the parton distributions at the starting scale and on the value of the strong coupling constant α_s. The ZEUS QCD fit, tuned to the same data from which the slopes have been determined, follows the x dependence of $dF_2/d\ln Q^2$ down

to lower values of Q^2. The flattening of the slope at $Q^2 \sim 1$ GeV^2 reflects the flat x-dependence of the gluon distributions determined from the ZEUS QCD fit at this Q^2 scale.

While in the pQCD regime the logarithmic Q^2 slope is sensitive to the gluon distribution, the x dependence of the structure function F_2 is related to the sea quark distribution. The fact that at $Q^2 \sim 1$ GeV^2 F_2 continues to rise with decreasing values of x is consistent with the x dependence of the singlet quark distribution obtained at these Q^2 values from the ZEUS QCD fit.

3 New experimental results

In order to reduce the background and the systematic error of the F_2 measurement in the transition region, ZEUS installed a tracker (BPT), consisting of two silicon microstrip detectors, in front of the Beam Pipe Calorimeter in 1997.

The BPT complements the information of the BPC for the reconstruction of the scattered positron and the measurement of the scattering angle. There are several advantages to using a tracker in front of the Beam Pipe Calorimeter:

- The tracker can be used to reduce the main source of background in the BPC analysis, due to neutral particles in the final state from photoproduction events misidentified as positrons. The reduction of the background allows extension of the kinematic coverage to higher values of y with respect to the 1995 analysis.
- With the BPT the scattering angle can be measured more precisely and independently of the knowledge of the interaction vertex; the F_2 measurement is thus less dependent on the efficiency of the vertex reconstruction and on the simulation of the hadronic final state in the Monte Carlo.
- The use of the BPT in the reconstruction of the track coordinates gives a better control of the fiducial volume cuts and of the position dependent corrections in the BPC energy reconstruction. The energy calibration, performed on 1997 data using kinematic peak events, determines the energy scale of the calorimeter to within $\sim 0.3\%$; the energy scale is uniform within $\pm 0.3\%$ over the entire active area of the detector.

The data taken with the BPT during six weeks at the end of the 1997 running period, corresponding to an integrated luminosity of 3.9 pb^{-1}, have been used to measure F_2. The kinematic region covered by this analysis is $0.045 < Q^2 < 0.65$ GeV^2 and $6 \times 10^{-7} < x < 1 \times 10^{-3}$, corresponding to $25 < W < 270$ GeV and $0.007 < y < 0.8$. The kinematic coverage has been extended to lower and higher y with respect to the 1995 BPC analysis. The lowest y bins overlap with the measurements of the E665 experiment.

For $y > 0.08$, the event kinematics are reconstructed with the electron method. At lower y, the y resolution is improved by combining positron and hadronic final state variables with the $e\Sigma$ method [26].

The simulation of ep events in this analysis makes use of two Monte Carlo generators: non-diffractive events are generated with DJANGO [24], while diffractive

– low mass and low multiplicity – events are generated with RAPGAP [25]. The two Monte Carlo samples are mixed in a proportion determined by fitting distributions of hadronic variables in data with a weighted sum of DJANGO and RAPGAP events.

The value of $R = F_L/(F_2 - F_L)$ is taken from the BKS model [27]. Due to the low Q^2 of this analysis, the effect of F_L is small, reaching at most 3% in few bins at high y and moderate Q^2.

The data are shown in Fig. 7, together with two fits (ALLM97 [13], DL98 [14]) which include the 1995 measurements, as well as with the original DL parameterization.

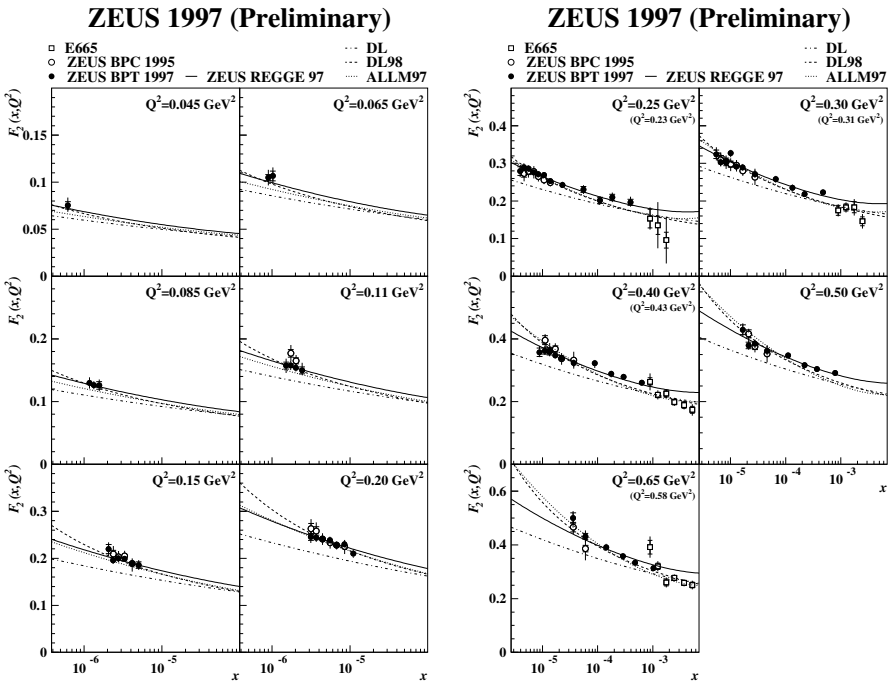

Fig. 7. F_2 as a function of x in bins of Q^2 from the BPT analysis compared with previous measurement from ZEUS (BPC 95) and E665 results

The average statistical error, including the statistical error of the Monte Carlo simulation, is 2.6%. The typical systematic error of 3.3% is similar to the statistical one and has been reduced by a factor 2 to 3 compared to the previous measurement.

The BPT F_2 data are converted to total $\gamma^* p$ cross sections using (1) and are shown in Fig. 8 as a function of Q^2 for different W bins. The measured cross sections for fixed W have been fitted to (4), with the values of the cross sections $\sigma_0(W^2)$ at $Q^2 = 0$ left as free parameters. The fit has a reasonable χ^2/dof of

1.3, taking into account statistical errors only; this indicates that the simplified GVDM model of (4) describes well the Q^2 dependence of the cross section.

The extrapolated cross sections σ_0 are shown in Fig. 9 as a function of the center of mass energy W; in the same figure the direct measurements from H1 [28] and ZEUS [29] and data from other experiments at low W [20] are also shown, and compared with the DL98 [14] and ALLM97 [13] parameterizations. The magnitude of the model dependence, estimated by extrapolating $\sigma_{tot}^{\gamma^* p}$ with the Q^2-dependence of DL, DL98 and ALLM97 parameterizations, is shown as a shaded band in Fig. 9.

A fit of the cross sections $\sigma_0(W)$ extrapolated from the BPT data, and of the low W measurements with the Regge-type form of (2) fixing $\alpha_{IR} = 0.5$, gives a value of the Pomeron intercept $\alpha_{IP} = 1.105 \pm 0.001(stat) \pm 0.007(sys)$.

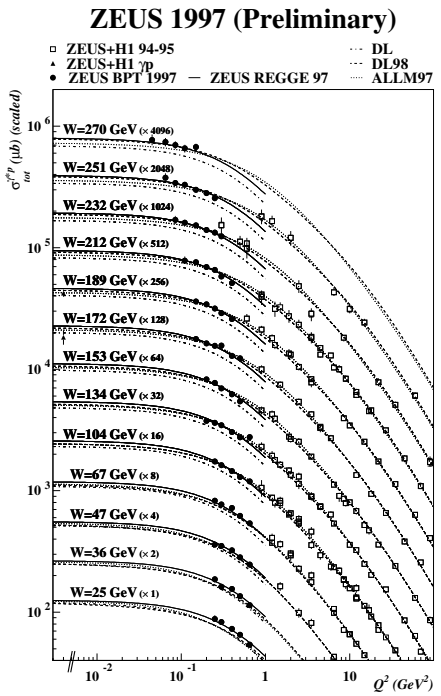

Fig. 8. $\sigma_{tot}^{\gamma^* p}$ versus Q^2 in bins of W from the BPT F_2 analysis and other measurements from ZEUS and H1

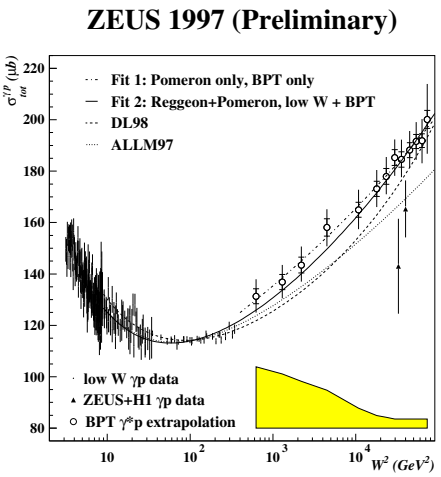

Fig. 9. Extrapolated and measured $\sigma_{tot}^{\gamma p}$ versus W^2. The curves are the ALLM97 and DL98 parameterizations and the result of the Regge fit described in the text

4 Conclusions

The HERA measurements of F_2 and $\sigma_{tot}^{\gamma^* p}$ at low Q^2 and x, in the transition region between DIS and the photoproduction limit, have been presented. The

data with $Q^2 < 0.65$ GeV^2 can be described by a simple GVDM and Regge-inspired parameterization, which however fails at higher Q^2. The rapid fall of F_2 at small x for $Q^2 > 1$ GeV^2 is described by NLO QCD fits.

The slopes $d\ln F_2/d\ln(1/x)$ at fixed Q^2 and $dF_2/d\ln Q^2$ at fixed x have been detemined from the HERA data. In the regime where pQCD is reliable, the behaviour of the slopes is compatible with the results of a NLO QCD fit.

References

1. H1 Collab., I.Abt et al.: Nucl.Phys. B **407** (1993) 515;
   H1 Collab., T.Ahmed et al.: Nucl. Phys. B **439** (1995) 471
2. ZEUS Collab., M.Derrick et al.: Phys.Lett. B **316** (1993) 412; Z.Phys. C **65** (1995) 379; Z.Phys. C **72** (1996) 399
3. H1 Collab., S.Aid et al., Nucl.Phys. B **470** (1996) 4; H1 Collab., C.Adloff et al.: Nucl.Phys. B **497** (1997) 3
4. ZEUS Collab., M.Derrick et al.: Z.Phys. C **69** (1996) 607; Z.Phys. C **72** (1996) 399
5. M.Glück, E.Reya and A.Vogt: Z.Phys. C **48** (1990); Z.Phys. C **53** (1992) 127; Z.Phys. C **67** (1995) 433
6. V.N.Gribov and L.N.Lipatov: Sov.J.Nucl.Phys. **15** (1972) 438, 675; L.N.Lipatov: Sov.J.Nucl.Phys. **20** (1975) 95; Y.L.Dokshitzer: Sov.Phys.JETP **46** (1977) 641; G.Altarelli and G.Parisi: Nucl.Phys. B **126** (1977) 298
7. A.D.Martin,R.G.Roberts and W.J.Stirling: Phys.Lett B **387** (1996) 419
8. A.Donnachie, P.V.Landshoff: Phys.Lett. B **296** (1992) 227
9. A.Capella, A.Kaidalov,C.Merino, J.Tran Thanh Van: Phys.Lett. B **337** (1994) 358
10. B.Badelek and J.Kwiecinski: Phys.Lett. B **295** (1992) 263
11. K.Adel, F.Barreiro and F.J.Ynduráin: FTUAM 96-39, HEP-PH.9610380
12. E.Gotsman, E.M.Levin and U.Maor: Phys.Lett B**425** (1998) 369
13. H.Abramowicz and A.Levy: DESY 97-251
14. A.Donnachie and P.V.Landshoff: Phys.Lett. B **437** (1998) 408
15. ZEUS Collab., J.Breitweg et al.: Eur.Phys.J. C **7** (1999) 609
16. H1 Collab., C.Adloff et al.: Nucl.Phys. B **497** (1997) 3
17. ZEUS Collab., J.Breitweg et al.: Phys.Lett B **407** (1997) 432
18. E665 Collab., M.R.Adams et al.: Nucl.Rev. D **54** (1996) 3006
19. J.J.Sakurai and D.Schildknecht: Phys.Lett. B **40** (1972) 121
20. D.O.Caldwell et al.: Phys.Rev.Lett. **40** (1978) 1222; S.I.Alekhin et al.: CERN-HERA 87-01 (1987)
21. NMC Collab., M.Arneodo et al.: Nucl.Phys. B **483** (1997) 3
22. BCDMS Collab., A.C.Benvenuti et al.: Phys.Lett. B **223** (1989) 485; Phys.Lett. B **237** (1990) 592
23. A.D.Martin et al.: Eur.Phys.J. C**4** (1998) 463
24. K.Charchula, G.A.Schuler and H.Spiesberger: Comp.Phys.Commun. **81** (1994) 381; H.Spiergerger, DJANGO6 version 2.4 - A Monte Carlo Generator for Deep Inelastic Lepton Proton Scattering including QED and QCD Radiative effects (1996)
25. H.Jung: Comp.Phys.Comm. **86** (1995) 147
26. U.Bassler and G.Bernardi: DESY 97-131
27. B.Badelek et al.: Z.Phys. C**74** (1997) 297
28. H1 Collab.,A.Aid et al.: Z.Phys. C **69** (1995) 27
29. ZEUS Collab.,M.Derrick et al.: Z.Phys.C **63** (1994) 391